A Novel Modelling Approach for Simulating Meltpool Movement in Laser-based Additive Manufacturing

Khuldoon Usman[*1], Henrik Kruse[2], Markus Niessen[3], Johannes Schleifenbaum[2], and Wolfgang Schulz[1,3]

[1]*Chair of Nonlinear Dynamics in Laser Manufacturing Processes, RWTH Aachen University, Steinbachstrasse 15, 52074 Aachen, Germany*
[2]*Chair of Digital Additive Production, RWTH Aachen University, Campus Boulevard 73, 52074 Aachen, Germany*
[3]*Fraunhofer Institute of Laser Technology, Steinbachstrasse 15, 52074 Aachen, Germany*
[*]*Corresponding author's e-mail: khuldoon.usman@nld.rwth-aachen.de*

Laser-based additive manufacturing (AM) processes, such as laser powder bed fusion (LPBF), involve the application of a laser beam to selectively melt and solidify powder particles to create three-dimensional objects. These processes are characterized by the dynamic movement of the laser beam over the powder bed, resulting in different geometries. Accurately predicting the thermal behavior within and around the meltpool location during laser beam movement is crucial for optimizing process parameters, predicting material properties, and ensuring structural integrity. Considering the high temperatures involved, the temperature cannot be determined easily through typical experimental means. Thus, the simulation of the temperature development is of key importance as it needs to capture the shape and size of the meltpool and also compute a physically valid temperature distribution within it. The movement of such a meltpool is conventionally simulated via moving heat sources rely on solving transient heat conduction equations, which are computationally expensive as well as complex algorithms for the calibration and movement of such a source. The goal of this work is to showcase a novel and versatile approach for simulating meltpool movement by representing it as a quasi-stationary instantaneous heat source through the projection of temperature. The method involves projecting the temperature field of the meltpool model onto a domain as boundary conditions for a steady-state heat conduction equation in every movement step. The meltpool model chosen is calibrated from experiments and accounts for capillary flow and depth dependent absorption and thus has been already validated in previous research. This model serves as a starting point for implementing an approximation of the heat source movement to be later used for a multi-scale model where information can be upscaled from this approach. Multi-scale models can then be used to capture such fine scale information yet making a computationally feasible model for the entire LPBF process which is then planned to be continued in further publications. The projection approach shows a stable and accurate development of temperatures and is computationally comparable to directly using a source function with parallel processing and comparable to other heat source models in literature.
DOI: 10.2961/jlmn.2025.01.2004
Keywords: additive manufacturing, meltpool modelling, heat source movement, thermal simulations

1. Introduction

One of the most popular manufacturing techniques in Additive Manufacturing (AM) is the Laser Powder Bed Fusion process which is widely use in the industry due to promising advantages such as better precision, higher processing speed, less material waste and considerable flexibility[1]. However, understanding all the physical phenomenon in such a manufacturing technique can be challenging for reasons such as the extremely fast moving laser beam, the significant temperature gradients near the energy source, the irregular dynamic effects of the meltpool and the overall complex developments of residual stresses that lead to unwanted deformations [2–4]. The process involves the moving of a laser over a layer of powder material in a pre-specified contour which makes up one slice of the final part on that layer[5]. The layer is moved in a sequential pattern for every layer of the powder material it works on and successive layers are then subsequently built up via repeated melting and solidification of the powder according to the predetermined contour for each layer. The laser usually moves in a repetitive linear fashion where each line of deposited energy and melted powder is called a track as shown in Figure 1. This technique is known as Laser Powder Bed Fusion (LPBF). The molten/liquid region is called the meltpool and it moves with the laser as more powder in front of the meltpool is melted and the melted pow-

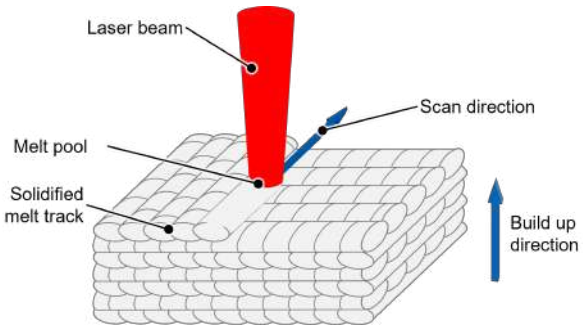

Fig. 1 Laser beam (heat source) moves in multiple tracks to cover the desired powder material in every layer.

der behind it eventually solidifies. Thus in one track, once steady state motion is achieved, the meltpool develops a well defined shape. It is the modelling of this meltpool that is a focus for many researchers because the liquid inside the meltpool has many dynamic effects occuring simultaneously which affect the temperature distribution around it[6–8]. The study and analysis of the temperature distribution around the meltpool is critical in determining build quality, optimum process parameters and controlling the aforementioned unwanted deformations.

Multi-scale models are becoming more and more popular for modelling laser based additive manufacturing processes due to the amount of complex phenomenon involved and the computational time needed to capture all small scale effects for a part level simulations. By incorporating phenomena at different length and time scales (from microstructure formation to part-level thermal and mechanical behavior), multi-scale models can capture both fine-grained details (such as melt pool dynamics) and macroscopic effects (such as residual stresses and distortion) in a computationally efficient manner [7]. These models also allow for repetitive communication between the different scales thus aiding in determining optimzed process parameters for desired effects [9]. However, even such models need some approximation and simplifications for the purpose of making the overall simulation practical and thus a number of simplifications have been implemented over time to reduce computation effort for the sake of having a holistic model. Multi-scale models often use techniques like spatial refinement (focusing computational resources on critical regions like the melt pool) or time-averaging (simplifying small-scale phenomena) to balance computational efficiency with accuracy [10]. Studies have shown how large scale thermal gradients have a bigger impact compare to micro-scale transient effects and thus averaging temperatures over part or layer section is computationally valid when determining overall residual stresses as long as the sharp thermal gradients are captured during the heating and cooling process[11, 12].

An accurate model is needed at the smallest scale i.e. at the level of the meltpool that can simulate the laser beam and meltpool movement and its interaction with the material for a complete thermomechanical problem. One of the main reasons why simulation of temperature around the meltpool is a key issue are the extremely large temperatures and temperature gradients in the vicinity of the meltpool. While the meltpool geometry is a quantity that can still be determined with experimental measurements, the temperatures are challenging to measure through conventional experimental means[13]. Therefore, these temperatures are determined through more technically rigorous and extensive experimental approaches[14, 15], as well as highly complex optical and thermal measurement equipment[16, 17] which can still generate unreliable results. Hence, the development of an effective and efficient model for meltpool is crucial in studying the temperature distribution. Moreover, it is more experimentally feasible to capture thermal history instead of instantaneous snapshots of temperature and the same temperature distribution can correspond to different meltpool shapes. Thus, it is meaningful to have a model which can recreate meltpool shapes from physical process rather than just experimental observation alone[18]. This model should also serve as the starting point of the simulation of an LPBF process by allowing for developing simulations for meltpool movement as well as for further multi-scaling strategies to allow for hatch, layer or whole part modelling. Movement of this meltpool model is normally simulated via well calibrated volume heat source models which require an empirical or optimization based approach to determine the parameters that describe the shape of such a heat source as well as the variation of flux to determine the temperature distribution.

2. Motivation

The aim is to recreate a physically valid temperature distribution as well as the meltpool boundary i.e. the melting isotherm such that it recreates the shape of the meltpool. The modelling process mainly consists of reproducing the heat content generated by the laser beam, the corresponding temperature distribution that is generated as well as the movement of the heat source itself. Researchers have used approximate analytical functions to approximate heat source geometries as there movement is relatively simple to simulate in Cartesian space such as the Gaussian or Goldak heat sources[4, 19–21]. However, in moving such analytical functions, challenges arise involving complex computations over the whole time domain[22–24]. There are other more effective ways of modelling the movement of such heat sources such as mesh-free methods but those require implementation of detailed and intensive algorithms that are not trivial[25–27]. Moreover, using a calibrated heat source (such as Goldak), usually means the geometric parameters of the source needed to be determined in advanced which is not only time consuming but does not always result in unique meltpool geometries. Different sets of process parameter combinations create similar meltpool widths and depths, but with different longitudinal lengths (along movement direction) and thus leading to different temperature distributions[28, 29]. Last but not the least, the effort needed for obtaining the optimum heat source shape parameters can be quite time intensive involving complex optimization strategies [4, 30] and must be re-calibrated for every change in process parameters[31, 32].

The article highlights the challenges of conventional modeling approaches that treat the melt pool as a stationary heat source and thus neglect the dynamic effects of melt pool motion. A novel method is presented that explicitly accounts for the melt pool motion while solving the heat conduction problem in the solid phase of the powder. This method uses a finite element method (FEM) and is based on a novel approach to define the melt pool shape and motion based on a physical understanding of the melt pool dynamics. The starting point for this approach is a process model of a meltpool already published by some of the authors. Unlike, a Goldak source this model predicts meltpool features without the need for prior calibration of a heat source. It focuses on reproducing meltpool shape and is based on a modelling strategy that captures absorption dependence on the angle of incidence and the meltpool depth as well as including potential flow around the capillary, all of which serve as boundary conditions to the heat conduction problem. The variations in meltpool depth are studied against the laser power and scan velocity for a single track[29, 33] to validate this meltpool model against

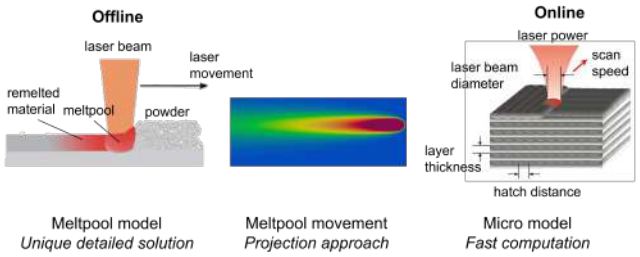

Fig. 2 Schematic showing the transition between a detailed offline model for the meltpool and a faster less complex online model for the movement.

experiments. This meltpool model serves as a starting point for the simulation of meltpool movement, highlighted in this work, which does not involve integration of the source function over time nor does it use calibrated heat sources with complex algorithms. Instead it uses the temperature distribution of the meltpool and projects it onto a domain where the heat conduction problem will be solved. In essence, temperatures and corresponding nodes/degrees-of-freedom (DOFs) are extracted from the model and are then projected onto a larger domain where the movement of the meltpool will be simulated. These projected temperatures are then applied as boundary conditions for the heat conduction problem to be solved on this domain. The heat conduction equation will be solved every time step after which the meltpool domain (and its corresponding data) are moved a certain amount and the whole process is repeated. The time steps will be sufficiently small such that the meltpool resembles a quasi-stationary instantaneous heat source in every time step thus preventing integration over time. This approach maintains the shape of the meltpool and since every meltpool model is unique and derived from the process itself, moving the meltpool model is always going to give a unique temperature distribution. This ensures that even during the movement of such a meltpool, the shape is not dependent on any free geometric parameters of some heat source but rather on the process parameters from which the meltpool is derived and therefore the accompanying temperature distribution will also be unique to the temperature distribution. This approach also allows to circumvent the complex computations in the meltpool model every time it is moved and simply recompute movement steps with the same model. This splits the modelling into an *offline* phase where the very complex computations need to be carried out only once i.e. in the meltpool recreation and a subsequent *online* phase for faster computation of temperature distribution during movement using the simpler projection approach. This then allows for faster computations at the level of multiple tracks or patches as showcase in Figure 2.

The use of constant meltpool temperature distributions does not always capture all the transient effects but studies have shown that use of similar quasi-steady-state models do not have significant influence on undesirable effects at the large scale, especially when predicting residual stresses at the part level. Rather, scan strategies have more promising effects and this technique allows for easier implementation and simulation of various scan strategies due to its simplicity with which improved and effective upscaling can be implemented [11, 34]. Additional studies have also showcased the computational benefits gained from this simplifications for rapid re-computation and optimization with respect to laser parameters [35]. Additionally, since this approach focuses on a significantly small scale (around the meltpool) compared to part level and serves to better approximate input quantities and loading/boundary conditions for a multi-scale model, thin wall effects can be ignored considering the domain is large enough to allow for sufficient diffusion of temperature far away from the meltpool. In further publications which focus on the larger scale, the authors plan to incorporate geometry based effects as well.

For the purposes of this work, all computations are carried out using the Python programming language. The libraries used for solving the partial differential equations are the FENICS open source computational libraries and its user interface called DOLFIN[36–39]. The Scipy library in Python is used to perform the interpolation[40] for the projection steps.

3. Methodology

A validated and self-consistent numerical model has already been developed by part of the authors as an extension to an already published capillary model for laser cladding[41]. It was modified to include the displacement flow around the capillaries as well as calibrated for absorption dependency. It also reproduces the solidification front in the longitudinal direction of movement.

The model solves the following heat conduction equation,

$$\rho\left(T\right)c_p\left(T\right)\frac{\partial T\left(t\right)}{\partial t}=\lambda\left(T\right)\left(\frac{\partial^2 T}{\partial x^2}+\frac{\partial^2 T}{\partial y^2}+\frac{\partial^2 T}{\partial z^2}\right), \quad (1)$$

where ρ, c_p, λ are the temperature dependent material properties: density, heat capacity and heat conductivity respectively. Additionally, the source term is defined by the laser beam where the intensity is fitted,

$$I(x,y\rightarrow r)= I_0\cdot\left(e^{\left(-f(n)\cdot\left(\frac{r}{r_0}\right)^n\right)}-e^{\left(-f(n)\cdot\left(\frac{r_{\text{Limit}}}{r_0}\right)^n\right)}\right), \quad (2)$$

where $I_0, f\left(n\right), r_{\text{Limit}}$ and r_0 are the fitting parameters to describe the laser radiation. The heat conduction is coupled with a boundary condition for energy absorption at the surface,

$$-\lambda\left(T\right)\frac{\partial T}{\partial z}\cdot\hat{n}=I_0\left(\vec{r}\right)\cdot P_L\cdot\alpha_0\cdot\alpha_{\text{key}}\left(d_{mp}\right), \quad (3)$$

where P_L, α_0 and α_{key} represent the laser power, basic absorption coefficient and keyhole absorption coefficient respectively. The key improvement in this model is that switching between conduction only mode and keyhole mode in the meltpool is not just determined through sufficient power and evaporation temperature but also is influenced by a change in the absorption characteristics which than affects the dimensions of the meltpool. The model also takes into account absorption dependence on the meltpool depth and a displacement flow in the capillaries. The melt pool flow is modeled using the potential flow theory, which simulates the displacement flow around the capillary. The streamlines of the melt pool flow are

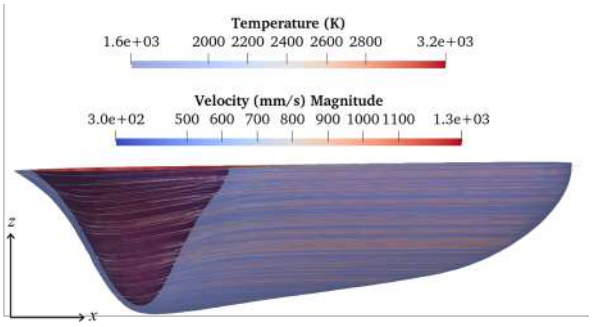

Fig. 3 Streamlines of the displacement flow around the capillary.

shown on the right in Figure 3. The comparison of meltpool depth for single track experiments with experiments showed good result for this meltpool model as highlighted in Figure 4. A side by side comparison for the model with an experimental meltpool cross-section is shown in Figure 5 . Incorporating angle dependent absorption as well as capillary flow, the model also better predicts the meltpool length against experiments in the longitudinal direction when compared to a Goldak source by more accurately predicting the solidification front[29, 33]. Thus, this meltpool model serves as a suitable starting point to showcase the projection approach.

3.1. Projection approach

The projection approach uses the aforementioned meltpool model as a starting point for movement simulation. As an example, one such simulated meltpool along with its given temperature distribution is shown in Figure 6. In the figure, the black and white lines represents the isotherms for the meltpool boundary i.e., melting temperature and the capillary boundary i.e., vaporization temperature respectively. For visualization purposes, the region inside the capillary has been filled with the max temperature since the values inside are of no consequence in the calculation i.e. there is no material inside.

The material parameters used for the problem are highlighted in Table 1. For the purposes of simplicity and computational acceleration, constant material properties are assumed. The meltpool domain is called the *source domain* $\Omega_s \subset \mathbb{R}^3$. On this source domain, the temperature distribution is defined as a finite element (FE) function T_s with a corresponding FE function space U_s such that $T_s \in U_s(\Omega_s)$. A larger domain for the solution is also defined henceforth as the *solution domain* Ω with a FE function for the *solved temperature* T_{sol} and the accompanying function space it will be defined on U_{sol}. T_s can then be interpolated into the solution domain at a given location where it is denoted as the *prescribed temperature* T_{pre}. The original source domain has an unstructured grid. Thus, the temperature values from T_s are first interpolated using an interpolater onto a structured grid before being projected on to the solution domain. The bounds of the source domain are used as the bounds of the structured grid which has a pre-defined spacing along each cartesian direction to define the hexahedral cell size. Once this interpolation is complete, the coordinates of the structured grid are scaled to unit spacing. The cells and coordinates of the solution

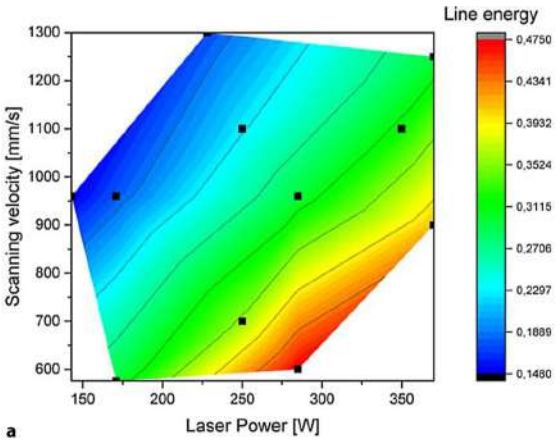

(a)

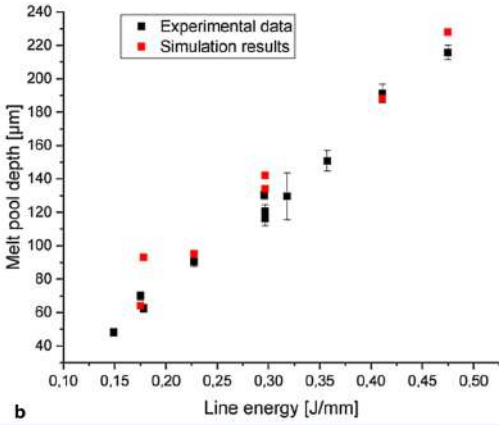

(b)

Fig. 4 (a) A line energy chart of the meltpool model for different combinations of scan velocity v_s and laser power P_L and (b) A comparison of meltpool depth with respect to different line energies in single tracks between the meltpool model and experiments[33].

domain are also scaled and transformed to the coordinate system of the unit scaled structured grid to determine which cells of the of the solution domain overlap with the structured grid. This is achieved via a mapping function between hexahedrals in the structured grid and the solution domain (also a structured mesh). Once these cells have been identified, all their corresponding DOFs and their Cartesian coordinates are determined. The corresponding temperature values in the structured grid are assigned to the *extracted* coordinates (which lie in the solution domain) via the mapping function and stored in an array. Then looping over the *extracted* DOFs, temperature values from the array are transferred to T_{pre}.

The criteria for choosing which values and DOFs from T_{pre} will be used as Dirichlet conditions is decided based on a certain temperature range. Only the meltpool is considered as the heat source and thus only those temperatures which lie between the melting point and the vaporization point should be considered. Once these DOFs and their corresponding temperature values have been identified, they can be simply applied as Dirichlet boundary conditions T_{bc} on the problem to be solved in the solution domain. The final heat conduction problem on the solution domain will look as such in the weak

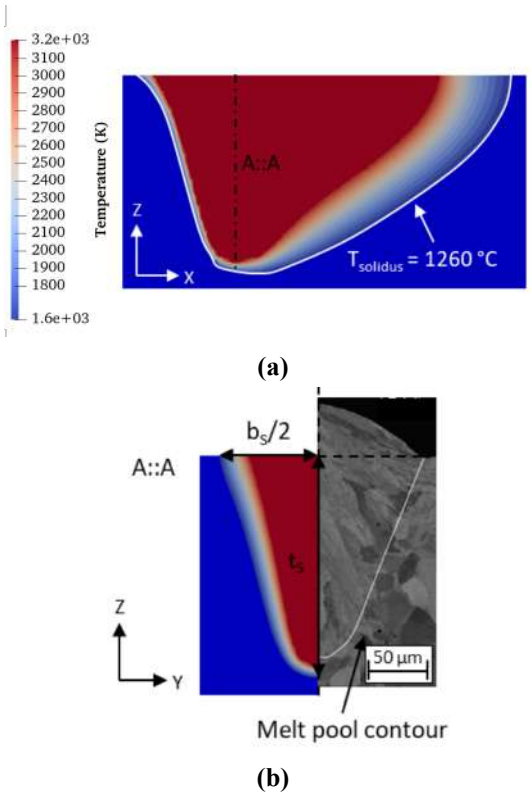

Fig. 5 (a) The meltpool model with the solidification boundary t_s highlighted and (b) A cross-sectional comparison with experiment showing half-width $\frac{b_s}{2}$ [29].

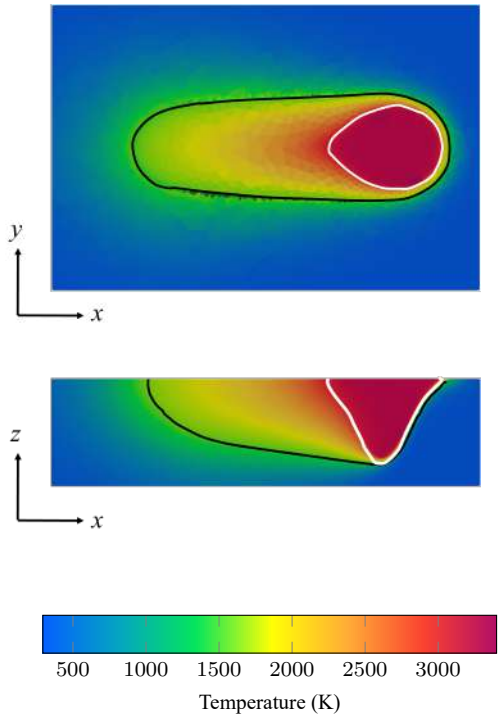

Fig. 6 The meltpool model highlighting the melting (black) and vaporization (white) isotherms.

Table 1 Material properties.

Property	Value (unit)	Ref
Thermal diffusivity (κ)	$4.538 \text{ x } 10^{-6}$ $\frac{m^2}{s}$	[29]
Ambient temperature (T_a)	294 K	[29]
Melting temperature (T_m)	1610 K	[29]
Vaporization temperature (T_v)	3270 K	[29]
Material density (ρ)	8000 $\frac{kg}{m^3}$	[29]
Specific heat capacity (c_p)	660 $\frac{J}{kgK}$	[29]
Thermal conductivity (k)	26 $\frac{W}{mK}$	[29]

Table 2 Parameters of source and solution domain.

Parameter	Value (unit)
Source domain	$0.6 \times 0.4 \times 0.15$ mm
Solution domain	$2.0 \times 1.2 \times 0.4$ mm
Source mesh	$50 \times 40 \times 30$
Solution mesh size	$200 \times 120 \times 40$
Relative beam shift (R_L)	0.5

form

$$\int_\Omega \rho c_p uv \, dV + \Delta t \int_\Omega k \nabla u \cdot \nabla v \, dV = \int_\Omega \rho c_p T_{old} v \, dV, \quad (4)$$

where $T = T_{bc}$ for those elements in Ω that contain the shortlisted DOFs, T_{old} is the temperature in the previous time step and the time step size is Δt. u and v are the test and trial functions respectively. Note that no explicit source term has been defined. Solving this heat conduction problem on the solution domain gives a distribution for the temperature in the whole domain for every time step. This is stored in T_{sol} which then becomes T_{old} for the next time step. Considering that T_{old} serves as the source for the problem, it is for this reason that the projected temperature range is chosen for T_{bc}, to make sure that the new temperature computed shows proper temperature diffusion away from the meltpool. After the temperature has been determined, the domain of the heat source is moved one increment forward such that,

$$T_s(x, y, z) = T_s(x + v_s \Delta t, y, z), \quad (5)$$

and then the whole process is repeated. Here, v_s is the scan velocity. Rotation of the source domain is achieved in a similar way. The parameters for the source and solution domain are shown in Table 2.

3.2. Time step size

The time step size Δt is automatically determined taking into consideration the movement velocity of the meltpool as well as the Courant–Friedrichs–Lewy (CFL) condition for advection-diffusion processes[42]. The value set for this condition is based on the solver scheme in use. The meltpool velocity is taken into account when explicitly restricting the

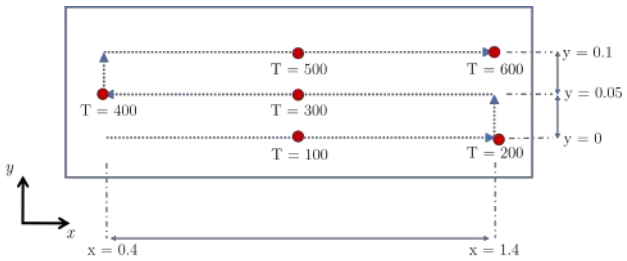

Fig. 7 The scan path of the meltpool movement.

relative shift of the beam R_L within one element in order to ensure the temperature variation is properly capture within the element's function space. Based on the smallest 3D element edge size in the mesh Δs and CFL parameter, a stable time step size Δt_Ω for the advection diffusion in the FE domain is determined,

$$\Delta t_\Omega = \text{CFL}\frac{(\Delta s)^2}{\kappa}, \tag{6}$$

as well as a time step size Δt_L for the relative beam shift,

$$\Delta t_L = R_L\frac{\Delta l}{v_s}, \tag{7}$$

where Δl is the smallest 2D element edge size only of the mesh surface where the laser beam is incident. Δt is then simply the smaller of the above two time step sizes i.e. $\Delta t = \min\{\Delta t_\Omega, \Delta t_L\}$. Thus, it is set to ensure that the meltpool movement for every timestep is small enough in every element such that the heat has sufficient time to diffuse irrespective of the movement velocity. This allows the meltpool to be represented as a *quasi-stationary* instantaneous source for every time step.

4. Results

To showcase the projection approach, the meltpool temperature distribution is moved along three tracks with a scan velocity based on conventional AM manufacturing parameters. The tracks' start and end points (in *mm*) are:

$$\begin{aligned}
&\text{Track 1}: \quad \text{Start} = [0.4, 0.0, 0.0], \quad \text{End} = [1.4, 0.0, 0.0]\\
&\text{Track 2}: \quad \text{Start} = [1.4, 0.05, 0.0], \quad \text{End} = [0.4, 0.05, 0.0]\\
&\text{Track 3}: \quad \text{Start} = [0.4, 0.1, 0.0], \quad \text{End} = [1.4, 0.1, 0.0]
\end{aligned}$$

where $[x, y, z]$ are Cartesian coordinates. At the end of a track, the heat source domain is now moved in the y-direction (instead of the x-direction) by the defined track spacing and then it is rotated 180° before being projected again onto the solution domain (in one time step). An illustration of this scan pattern is shown in Figure 7. T is the time step for which snapshots are shown in Figure 8 as the meltpool moves in the solution domain along the given scan pattern. The domain has been cropped for better visibility in the area of interest.

After a certain number of time steps, the meltpool shape is still retained and the temperature distribution is clearly well established behind it. The benefit here is that the exact meltpool shape is being moved without having to recalculate the temperature inside of the meltpool. As long as the time step size is properly adjusted to account for the velocity of the laser beam as well as for stable advection-diffusion, the meltpool maintains its steady state shape leading to a more reliable temperature distribution. Figure 9 shows the cross sectional view into the depth of how the meltpool moves along the first track and its temperature dispersion.

Another aspect showcased is the flexibility with which any meltpool distribution can be moved. Different process parameters combinations can lead to different meltpool shapes and moving all of them is very straightforward since only the source domain changes and the rest of the approach remains the same. Multiple meltpool models for different combinations of laser power and velocity were developed and a comparison of their movement via the projection approach is showcase in Figure 10. Since the different meltpools are all unique in their distribution, the challenge highlighted by Pittner[28] is overcome; namely that different combinations of the free goemetric parameters of the Goldak heat source can lead to similar meltpool models (thus not giving a unique temperature distribution for each meltpool). This is because, in projecting and moving individual meltpool models, there are no free parameters to consider or calibrate.

4.1. Moving arbitrary temperature distributions

Since this approach focuses on projecting and interpolating the temperature distribution of the meltpool, movement of any sort of temperature distribution can be studied using this technique. Instead of extracting a temperature distribution from an imported mesh, any spatially defined temperature function can be moved in this manner by defining it as a Python function and interpolating it into an FEM function using DOLFINx routines. Figure 11 showcases the use of a Gaussian temperature function being moved using this approach. The flexibility of this approach allows for different kind of stationary temperature distributions to be moved and tested. Incorporating a moving heat source is also straightforward. Since there is no temperature to project, T_{bc} is not needed (unless other boundary conditions are defined) and the source function can be incorporated easily on the right side. Movement of the source itself is then again represented as a quasi stationary heat conduction problem (albeit with no projected temperature boundary condition T_{bc} this time) based on the time step Δt such that temperature dispersion is physically valid. Moving a source function directly is faster to compute since no projection/interpolation is needed. Therefore, one drawback of the projection approach is that it needs to be made more computationally efficient. The use of parallel computing routines and multi-core computers aid in overcoming this disadvantage.

4.2. Parallel computations

Considering that this apporach requires the update of the boundary conditions in every time step, the left hand side of the equation is constantly being updated which is computationally more challenging that just changing the right hand side (in case of a source function) in every time step. However, the simulation of the projection approach is made computationally less challenging through the use of the *message passing interface* (MPI) for parallel computing which has a built in Python module integrated it into the DOLFINx libraries[43–45]. This allows for considerable speed up of the

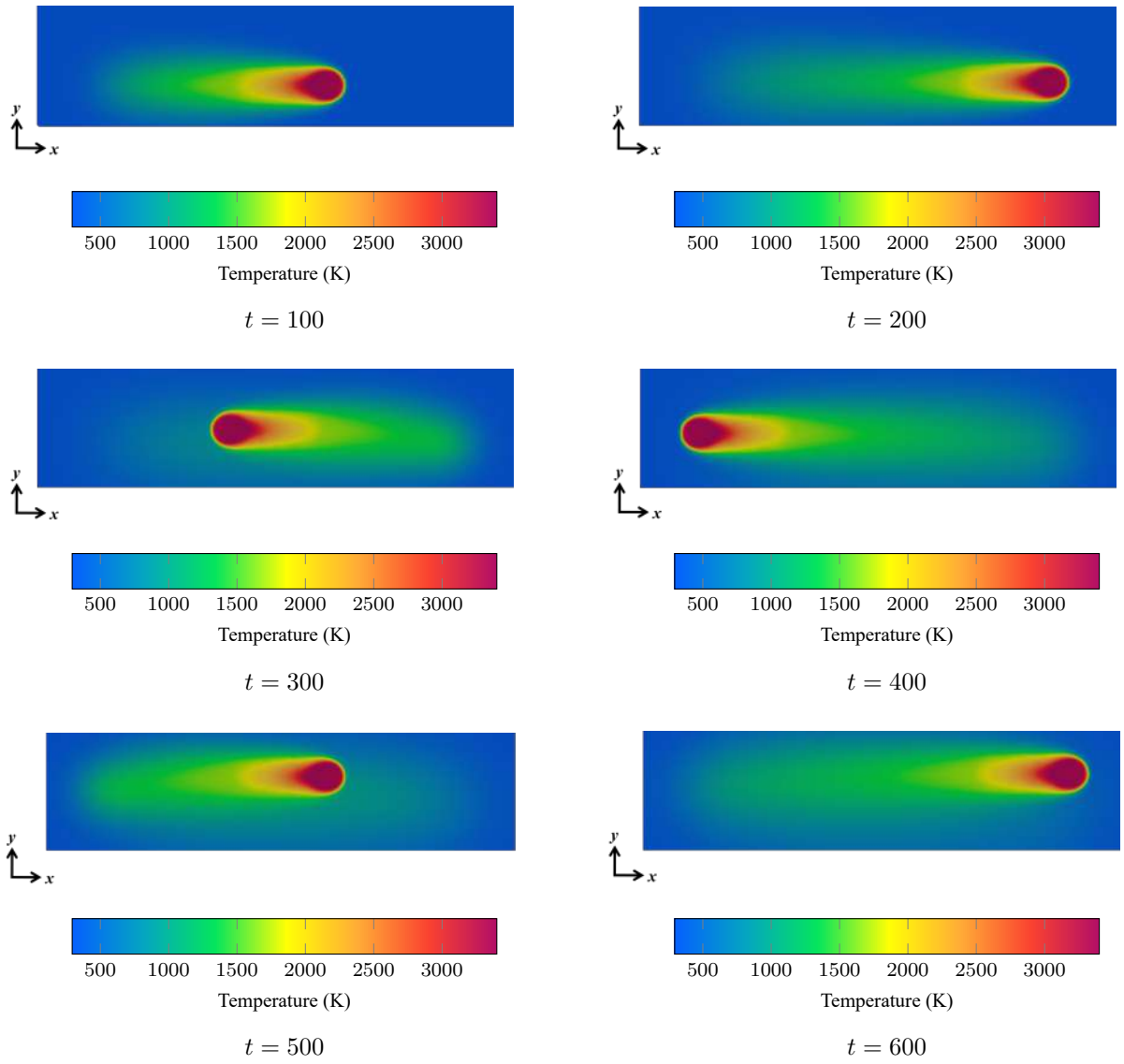

Fig. 8 Snapshots of the simulated meltpool movement for different time steps t along the three track scan pattern.

running simulation using multiple processors as highlighted in Figure 12. For comparison, the total DOFs were fixed in each case at 499041 in the solution domain. The graph in part (a) shows time taken for a single computational step with different processors. Using 1 processor (first data point) means no MPI is used. The graph in (b) shows the computational time with more than 1 processor as a fraction of total time using just 1 process (hence it starts from 2 processors). So value of 58% would mean that with this number of processors the computational time was 58% as long as the time taken when no MPI i.e. 1 processor is used. The time mentioned is the *real* or *wall-clock* time (as opposed to *sys* time or *user* time) since we have multi-threaded computation. The blue curve showcase the times for the approach involving the meltpool projection and the red curve shows when a analytical temperature function is projected. Additionally, direct movement of a source function (source term on right hand side of problem) is also compared with the green curve. Since projecting a meltpool or projecting a temperature function both gain similar advantages, when multiple processors are used, their curves are nearly identical. On the other hand, moving a source function is considerably faster since the projection step is skipped altogether. However, carrying out the computations in parallel clearly reduces the absolute time gap between the use of the temperature projection approach and the one with using a source function i.e. if 16 processors are used the projection approach computes a step in approximately $0.74 - 0.75$ seconds in the case of both a projected meltpool or a projected temperature function whereas the source function computes it in 0.099 seconds (the drop is logarithmic). While this is still a noticeable difference, the projection approach saves immense time and effort because the source function approach requires considerable effort in the initial calibration of its free geometric parameters (which is to be done every time process parameters are changed). Moreover, when coupling this heat conduction problem to a mechanical problem, the time taken for the mechanical computation step normally is much greater than the heat conduction step thus

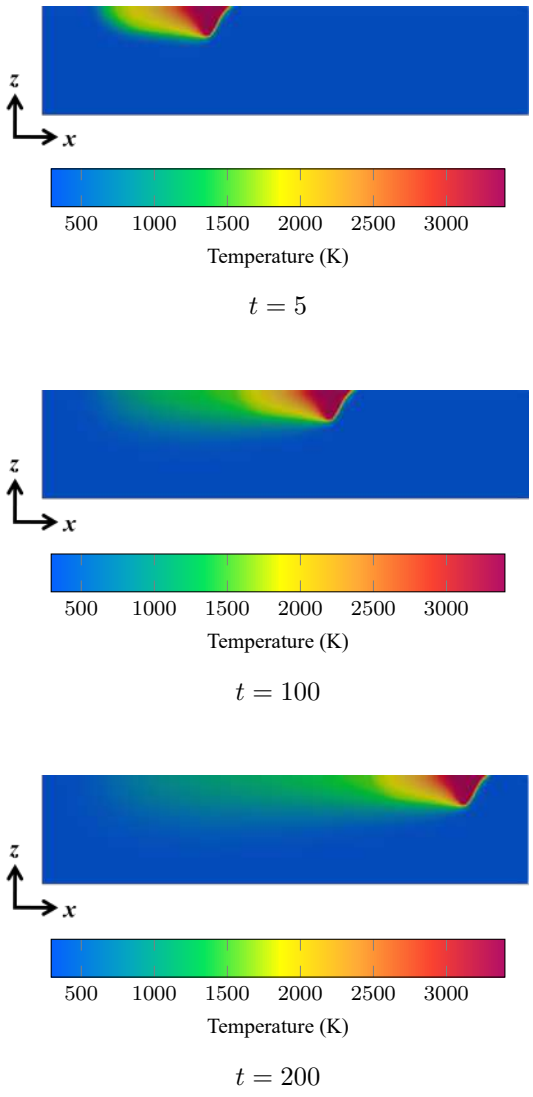

Fig. 9 Sideview of the simulation of the meltpool movement along the first track.

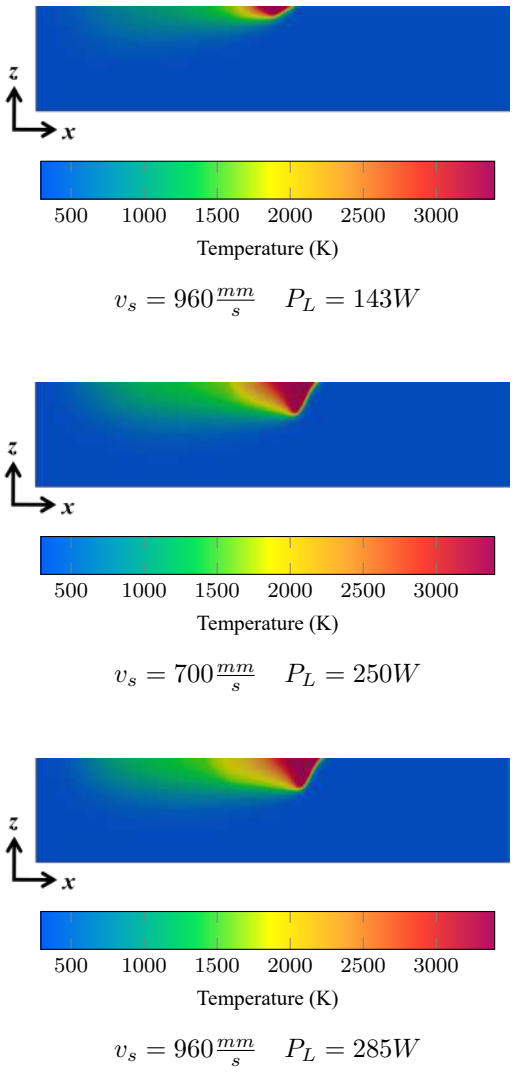

Fig. 10 A sideview of the movement of meltpool models for different combinations of laser power P_L and scan velocity v_s.

making the time difference between both approaches less of a dominant factor.

It can be seen that as soon as 24 processors are used, all approaches take longer than with 16 processors. This is because, increasing the number of processors does not scale proportionally with computation time due to the portion of the program to be conducted in serial as well as the additional computational effort that is needed for communication between multiple processors[46, 47]. This additional communication adds overhead on the processors that than slows down the computation since more time is now needed to actually share information between processors rather than computing the solution.

4.3. Comparison

In comparisons with other similar heat source or meltpool models, good agreement was found between others' work and the projection approach's results. Ross *et al.* developed a heat source model, calibrated using optimization techniques, that showed a good fit to their experimental results in predicting the meltpool boundary[4]. Thus, their approach was used as a comparative case for comparing the temperature variation. Only outside the meltpool is the comparison made since they fix the temperature to melting temperature on the inside (only for visualization) and the same is done for the projection approach. This comparison is illustrated in Figure 13. As per the qualitative distribution of temperature, the comparison shows that using the projection approach gives a similar temperature distribution while maintaining the meltpool shape and boundary without having to compute it from a calibrated heat source model. Granted, a meltpool model is needed to begin with but movement of the model is easier to implement and its stability is well established compared to a calibrated heat source model. It also saves on the calibration effort needed each time a new set of process parameters is used.

The material properties used by Ross *et al.* are different however and the comparison is limited to conduction only meltpool mode which differs from a keyhole meltpool where

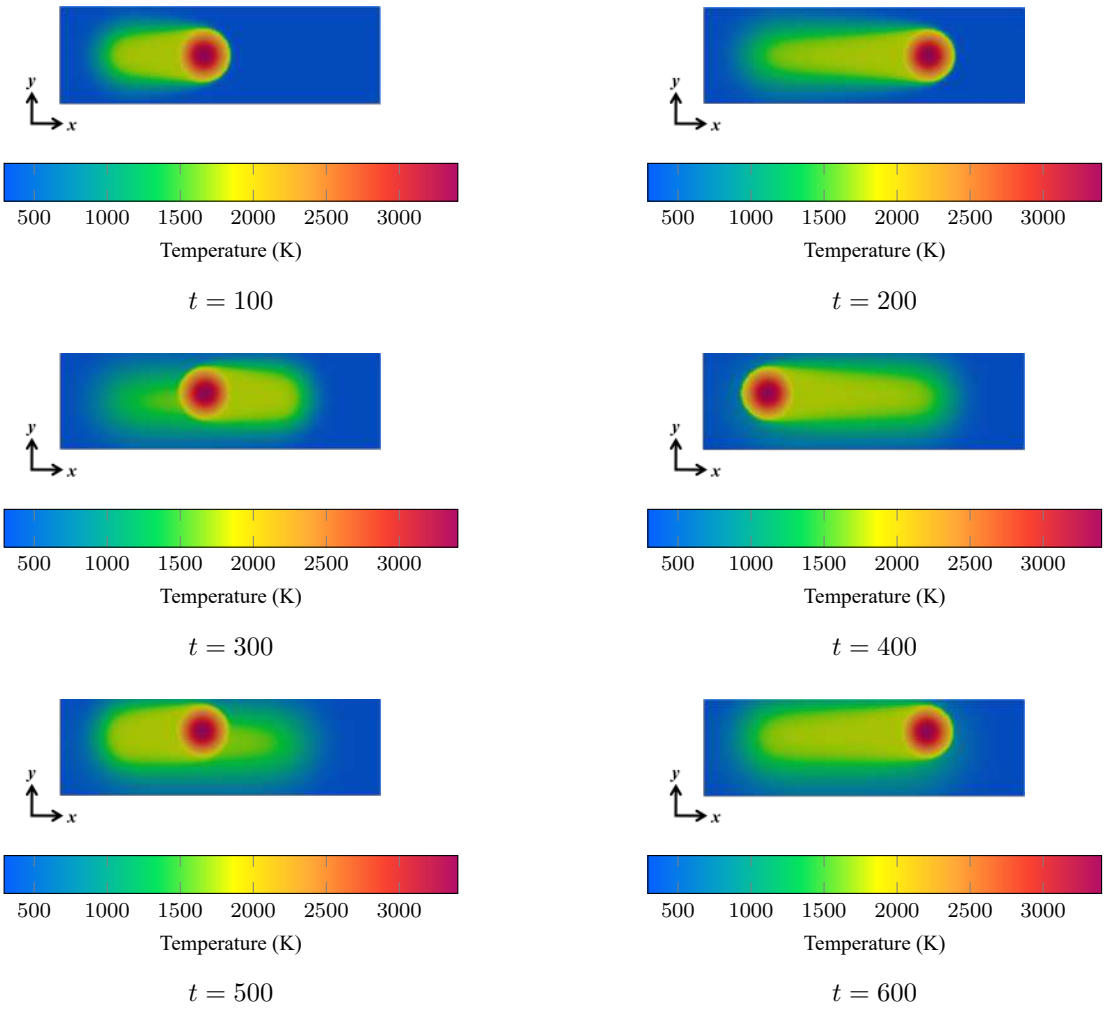

Fig. 11 Simulation of movement of a Gaussian temperature function along the three track scan pattern.

dynamics effect cannot be easily disregarded simply on the assumption of a steady state and as such calibration is needed to be done differently (due to other factors such as laser beam movement in the meltpool and depth dependent absorption etc.). Shahabad *et al.*[19] used an iterative procedure to calibrate a conical heat source which they used to study the meltpool dimensions as well as the temperature development and its influence on the micro-structure. Their model allowed for good prediction of meltpool dimensions in comparison to their experiments. The comparison of their approach with the projection approach is shown in Figure 14. As is the case with the approach by Ross *et al.*, the comparison with Shahabad *et al.* is limited to conduction only meltpool regime.

The key aspect in these comparisons is not the direct quantitative comparison between the projected meltpool and other researchers' heat source models. This will differ due to different process and material parameters. The main takeaway here is to observe the qualitative comparison and showcase that the projected meltpool approach maintains a physically valid temperature distribution for single tracks that is similar to what other researchers have modelled using other more traditional yet challenging approaches.

5. Discussion

The projection method offers an efficient and flexible alternative to traditional approaches for simulating the melt pool movement in laser powder bed fusion. It offers advantages in terms of computational effort, calibration requirements and flexibility in the geometry of the heat source. However, it is important to consider the potential drawbacks in terms of the accuracy of the external temperature field and the ability to model complex melt pool phenomena.

5.1. Key advantages

The projection method offers various advantages for the simulation of the melt pool movement in additive manufacturing with laser powder bed fusion:

No complex calibration: the projection method does not require complex calibration for each change in process parameters. Instead, an external set of temperatures, e.g. a melt pool model, is projected onto a solution domain and shifted at each time step to simulate the movement of the heat source. This makes the approach parameter-free and avoids complex analytical calculations or elaborate algorithms.

Flexibility in geometric parameters: The projection method can handle different geometric parameters of heat source models. This is an advantage over calibration-based approaches, which are often limited to certain geometries.

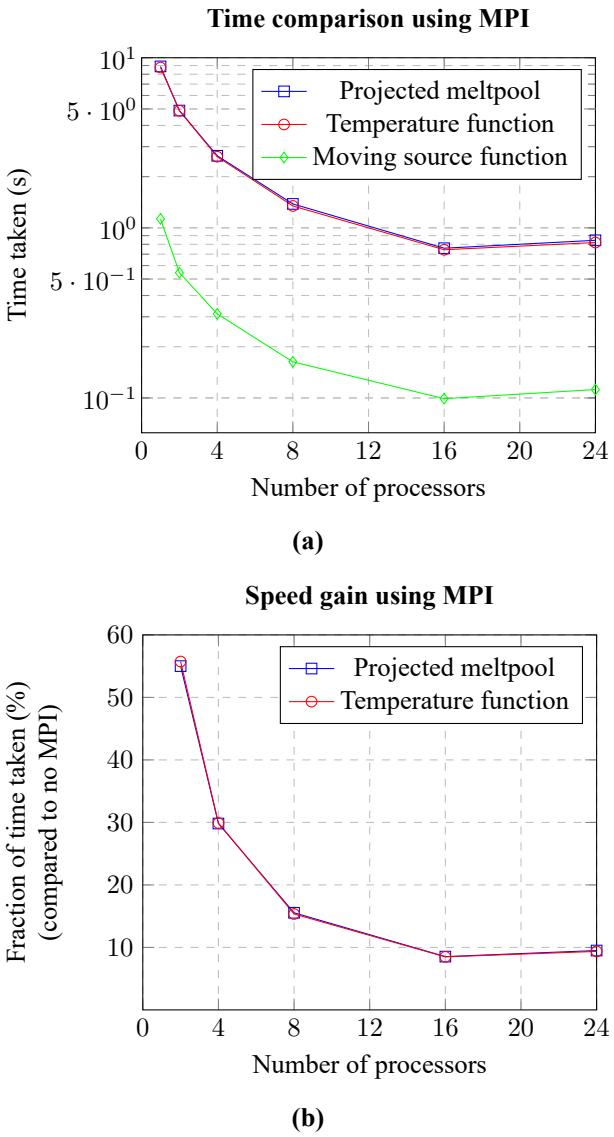

Fig. 12 Comparing the projection approach vs a source function using multiple processers in (a) and the relative speed up of the projection approach with MPI in (b).

The use of an external temperature field eliminates the need to calibrate the heat source and greatly simplifies the simulation process. The flexibility is relevant as different geometries can lead to identical melt pool dimensions and vice versa.

More efficient calculation: The projection method is computationally more efficient than using a moving heat source function. This is because it minimizes the time-dependent heat conduction resulting from the dynamic movement of the heat source. Instead of modeling the heat source directly, the temperature field is simply shifted at each time step. This approach simplifies the calculations and shortens the calculation times. Additonally, a lot computational time is saved from having to calibrate and optimize the heat source from the experimental results in order to have a unique source shape. The advantage becomes clearer when several processors are used to parallelize the calculations.

Explicit computation: the projection method projects an external temperature field, such as a melt pool model, directly

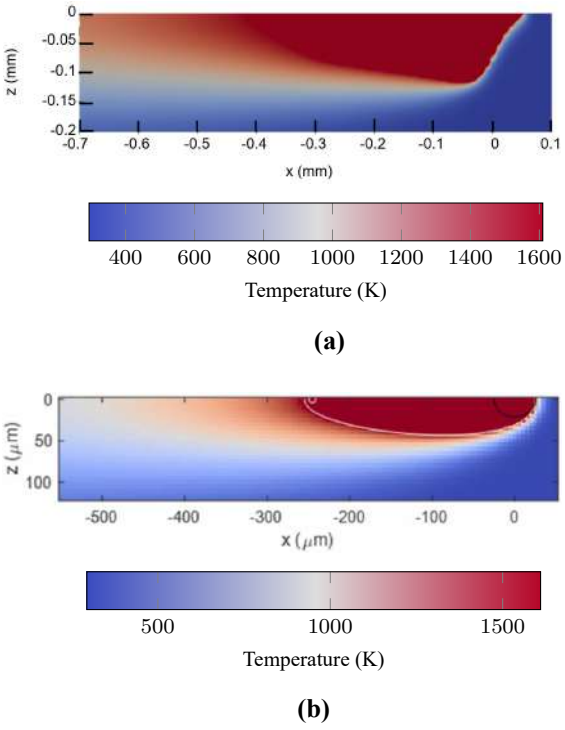

Fig. 13 Comparison between temperature distribution of (a) Projected meltpool model (b) Calibrated heat source from Ross *et al.*.

onto the solution domain and shifts it at each time step. This approach avoids the need to model the heat source directly and explicitly enforces the meltpool shape for a certain laser velocity and power to ensure physically reasonable temeprature computation.

Comparability with other methods: The simulation results of the projection method are comparable with those of other approaches for simulating the melt pool movement.

5.2. Other considerations

The parameters taken into account when simulating the melt pool movement depend on the model used. In general, the most important parameters include:

Laser power: The laser power affects the amount of energy introduced into the weld pool, which directly affects the size and shape of the weld pool.

Scanning speed: The scanning speed influences the time the laser remains at a certain point, which also affects the size and shape of the weld pool.

Powder material: The physical properties of the powder material, such as thermal conductivity, density and melting temperature, play an important role in determining the behavior of the weld pool.

Ambient temperature: The ambient temperature can influence the cooling rate of the melt pool, which affects the resulting microstructure.

In addition, the novel model presented in the sources takes the following parameters into account:

Temperature distribution: the model uses an external set of temperatures, e.g. a melt pool model, as input. Movement of the heat source: The movement of the heat source

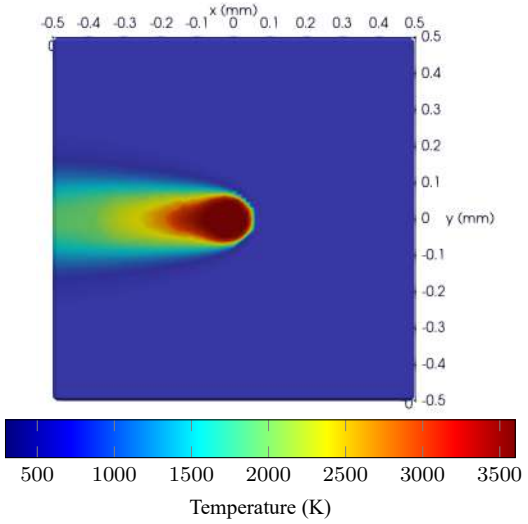

(a)

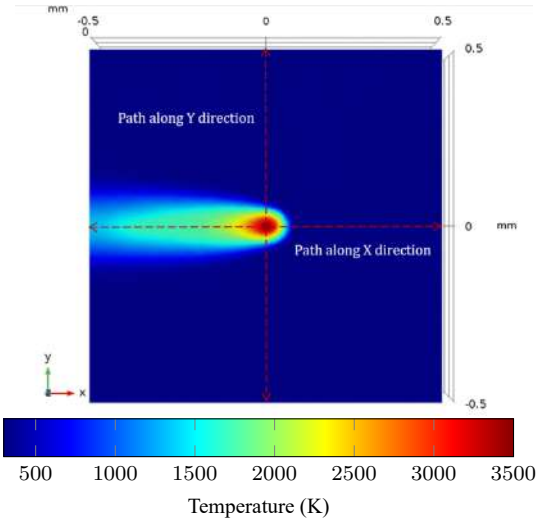

(b)

Fig. 14 Comparison between temperature distribution of (a) Projected meltpool model (b) Calibrated heat source from Shahabad *et al.*.

(laser beam) is explicitly modeled by shifting the temperature distribution at each time step.

Time step size: The time step size is automatically determined taking into account the velocity of the heat source and the stability conditions of the numerical scheme.

What could be useful for future researchers to consider is that this method provides researchers with a tool to simulate melt pool motion in additive manufacturing processes more accurately and efficiently. The knowledge gained can be then used to determine the energy and strain distribution for various scanning strategies for a multi-scale mode to optimize process parameters and improve the quality of additively manufactured parts. Due to the computational advantages of the method, researchers can simulate more complex scenarios such as multi-track or patch processes as well as rapid simulation of multiple material variations that would be difficult to tackle using conventional methods. Additionally, the presented method can be coupled with mechanical models to predict the mechanical properties and resulting microstructure of additively manufactured parts.

The accuracy of the simulation depends directly on the accuracy of the external temperature field used, which is often obtained from experimental data. If the external temperature field does not accurately reflect the actual temperature distribution in the melt pool, the simulation may provide inaccurate results but this is precisely why the already validated and detailed stabilized meltpool model is used as a starting point for the projection approach which ensure an accurate but complex simulation of all the necessary material and absorption dependent factor but is not feasible for modelling the entire movement of the meltpool (only sufficient until meltpool stabilization is reached). Nonetheless, the use of constant material properties during the projection and movement phase in this approach is a limitation which affects the accuracy of the temperature distribution during movement. The projection of a predefined temperature field also may present difficulties in capturing complex phenomena in the melt pool such as evaporation effects.

6. Conclusion and Outlook

The focus of this work was to introduce a novel approach to simulate the movement of heat sources in the laser based additive manufacturing process. The key outlines of this work are:

- Project an external set of temperatures from a source domain, such as a meltpool model, onto a solution domain
- Solve the stationary heat conduction problem in the solution domain with the projected temperatures as boundary conditions in every timestep
- Control the time step size to control the heat source movement in every element in order to maintain stable heat diffusion
- Based on the source velocity and timestep size, translate the external set of temperatures a certain increment and repeat the process to simulate movement

This method is used because it offers a number of advantages over other approaches to simulating melt pool motion:

- It does not require complex analytical calculations or complex algorithms to solve the heat conduction problem
- It does not need to be recalibrated for each change in process parameters
- It can generate different geometric parameters of heat source models, which is not the case with other methods that require calibration for each change.
- The method uses the actual heat source velocity and time step size to shift the heat source. - This allows the method to minimize the time-dependent heat conduction that results from dynamic motion.

In addition to these advantages, the computational complexity of this approach is relatively low. This makes it a

viable option for simulating the melt pool motion in real time, which can be beneficial for the optimization of laser powder bed fusion processes. The simulation results show that the projection approach is comparable to other approaches for simulating the melt pool motion. However, the approach is computationally more efficient, especially when using multiple processors. This makes it a promising approach for the simulation of melt pool motion in more complex scenarios, such as the simulation of multiple tracks or patches. In summary, the presented method provides researchers with a powerful tool for the simulation and analysis of melt pool motion in additive manufacturing processes due to its parameter-free nature, flexible geometry handling, efficient computation and parallelization capability.

For the future, the structure of the computations are planned to be more distributed such that even faster computation times can be achieved for the same number of processors. This is also beneficial for simulation of multiple layers or tracks on top of each other which is also planned as part of future publications of an overall comprehensive yet efficient multiscale model for the entire LPBF process. Additionally, even though the starting meltpool model incorporates temperature dependent material properties, the solution of the heat equation during projection and movement does not since it is just studying bulk material in this phase. Temperature dependent material properties will be studied in order highlight the transition between powder and solid during the implementation of this technique. Likewise, geometry effects e.g. thin wall geometries are to be studied on large scale.

The method is also used to predict the mechanical properties and resulting microstructure of additively manufactured parts. For this purpose, the temperature-controlled melt pool model will be coupled to a mechanical model. This will also allow to study the development of plasticity in the vicinity of the meltpool location. This will also be beneficial for the next research phase in which a multi-scale model will be developed using the results of this work for complete part level simulation of the LPBF process which will make it possible to better understand the influence of process parameters on the properties and microstructure of additively manufactured parts. The multi-scale model that follows from this can then be used to be better predict residual stresses and optimize parameters accordingly.

Acknowledgment

Funded by the Deutsche Forschungsgemeinschaft (DFG, German Research Foundation) under Germany's Excellence Strategy – EXC-2023 Internet of Production – 390621612. Also, co-funding provided by the Deutsche Forschungsgemeinschaft (DFG, German Research Foundation) — 418105836. Additionally, the insightful and fruitful discussions with Christian Heinigk and Jonas Zielinski are greatly appreciated.

References

[1] P. M. Gopal, V. Kavimani, K. Gupta, and D. Marinkovic: Micromachines, 14, (2023) 261.

[2] C. Weingarten, D. Buchbinder, N. Pirch, W. Meiners, K. Wissenbach, and R. Poprawe: J. Mater. Process. Technol., 221, (2015) 112.

[3] P. Bidare, I. Bitharas, R. Ward, M. Attallah, and A. Moore: Acta Mater., 142, (2018) 107.

[4] A. Ross, I. Bitharas, K. Perkins, and A. Moore: Addit. Manuf., 60, (2022) 103267.

[5] W. Meiners, K. Wissenbach, and G. Andres: German Patent DE19649865C1 (1998).

[6] C. Zhao, K. Fezzaa, R. W. Cunningham, H. Wen, F. De Carlo, L. Chen, A. D. Rollett, and T. Sun: Sci. Rep., 7, (2017) 3602:1.

[7] S. A. Khairallah, A. T. Anderson, A. Rubenchik, and W. E. King: Acta Mater., 108, (2016) 36.

[8] I. Bitharas, N. Parab, C. Zhao, T. Sun, A. D. Rollett, and A. J. Moore: Nat. Commun., 13, (2022) 2959.

[9] N. E. Hodge, R. M. Ferencz, and J. M. Solberg: Comput. Mech., 54, (2014) 33.

[10] J. Fish: "Multiscale Methods: Bridging the Scales in Science and Engineering", (OXFORD UNIV PR, 2009) 3.

[11] P. Mercelis and J.-P. Kruth: Rapid Prototyp. J., 12, (2006) 254.

[12] E. R. Denlinger, V. Jagdale, G. Srinivasan, T. El-Wardany, and P. Michaleris: Addit. Manuf., 11, (2016) 7.

[13] A. Vest, D. St-Pierre, S. Rock, A. Maniatty, D. Lewis, and S. Hocker. "Thermocouple Temperature Measurements in Selective Laser Melting Additive Manufacturing". English. Technical Memorandum 20220002988. National Aeronautics and Space Administration, 2022.

[14] S. Hocine, H. Van Swygenhoven, and S. Van Petegem: Addit. Manuf., 37, (2021) 101747.

[15] P. Scheel, P. Markovic, S. Van Petegem, M. G. Makowska, R. Wrobel, T. Mayer, C. Leinenbach, E. Mazza, and E. Hosseini: Addit. Manuf. Lett., 6, (2023) 100150.

[16] B. Lane, J. Heigel, R. Ricker, I. Zhirnov, V. Khromschenko, J. Weaver, T. Phan, M. Stoudt, S. Mekhontsev, and L. Levine: Integr. Mater. Manuf. Innov., 9, (2020) 16.

[17] B. Lane, S. Moylan, E. Whitenton, and L. Ma: Rapid Prototyp. J., 22, (2016) 778.

[18] J. Zielinski, H. Kruse, M.-N. Bold, G. Boussinot, M. Apel, and J. H. Schleifenbaum: International Joint Conference on Enhanced Material and Part Optimization and Process Intensification. (2021) 113.

[19] S. I. Shahabad, Z. Zhang, A. Keshavarzkermani, U. Ali, Y. Mahmoodkhani, R. Esmaeilizadeh, A. Bonakdar, and E. Toyserkani: Int. J. Adv. Manuf. Technol., 106, (2020) 3367.

[20] A. Hussein, L. Hao, C. Yan, and R. Everson: Mater. Des., 52, (2013) 638.

[21] A. Ilin, R. Logvinov, A. Kulikov, A. Prihodovsky, H. Xu, V. Ploshikhin, B. Günther, and F. Bechmann: Phys. Procedia, 56, (2014) 390.

[22] N. T. Nguyen, A. Ohta, K. Matsuoka, N. Suzuki, and Y. Maeda: AWS Weld. J., 78, (1999) 265s.

[23] J. Winczek: Int. J. Heat Mass Transf., 53, (2010) 5774.

[24] T. Flint, J. Francis, M. Smith, and A. Vasileiou: Int. J. Therm. Sci., 123, (2018) 140.

[25] S. Chen and Q. Duan: Comput. Mater. Sci., 183, (2020) 109911.

[26] Z. Hu and Z. Liu: Adv. Math. Phys., 2020, (2020) 6067854.

[27] X. Zhang and H. Xiang: Int. J. Heat Mass Transf., 84, (2015) 729.

[28] A. Pittner. "A Contribution to the Solution of the Inverse Heat Conduction Problem in Welding Simulation". P.hD Thesis. Berlin: Technische Universität Berlin, 2012.

[29] J. Zielinski. "A holistic approach to understand laser additive manufacturing from melt pool to microstructure". P.hD Thesis. Aachen: RWTH Aachen University, 2022.

[30] M. Kusano, H. Kitano, and M. Watanabe: J. Mater., 14, (2021) 127.

[31] M. Bayat, W. Dong, J. Thorborg, A. C. To, and J. H. Hattel: Addit. Manuf., 47, (2021) 102278.

[32] M. Kusano and M. Watanabe: Integr. Mater. Manuf. Innov., 13, (2024) 288.

[33] J. Zielinski, G. Boussinot, G. Laschet, M. Apel, and J. H. Schleifenbaum: Berg- Huettenmaenn Monatsh, 165, (2020) 175.

[34] J. Robinson, I. Ashton, P. Fox, E. Jones, and C. Sutcliffe: Addit. Manuf., 23, (2018) 13.

[35] S. Bontha, N. W. Klingbeil, P. A. Kobryn, and H. L. Fraser: Mater. Sci. Eng. A, 513-514, (2009) 311.

[36] A. Logg, K.-A. Mardal, and G. Wells: "Automated Solution of Differential Equations by the Finite Element Method", (Springer, 2012) 173.

[37] A. Logg and G. N. Wells: ACM Trans. Math. Softw., 37, (2010) 20:1.

[38] M. S. Alnæs, A. Logg, K. B. Ølgaard, M. E. Rognes, and G. N. Wells: ACM Trans. Math. Softw., 40, (2014) 9:1.

[39] M. W. Scroggs, J. S. Dokken, C. N. Richardson, and G. N. Wells: ACM Trans. Math. Softw., 48, (2022) 18:1.

[40] P. Virtanen, R. Gommers, T. E. Oliphant, M. Haberland, T. Reddy, D. Cournapeau, E. Burovski, P. Peterson, W. Weckesser, J. Bright, S. J. van der Walt, M. Brett, J. Wilson, K. J. Millman, N. Mayorov, A. R. J. Nelson, E. Jones, R. Kern, E. Larson, C. J. Carey, İ. Polat, Y. Feng, E. W. Moore, J. VanderPlas, D. Laxalde, J. Perktold, R. Cimrman, I. Henriksen, E. A. Quintero, C. R. Harris, A. M. Archibald, A. H. Ribeiro, F. Pedregosa, P. van Mulbregt, and SciPy 1.0 Contributors: Nat. Methods., 17, (2020) 261.

[41] N. Pirch, S. Linnenbrink, A. Gasser, K. Wissenbach, and R. Poprawe: J. Laser Appl., 29, (2017) 022506.

[42] R. Courant, K. Friedrichs, and H. Lewy: Math. Annal., 100, (1928) 32.

[43] E. Gabriel, G. E. Fagg, G. Bosilca, T. Angskun, J. J. Dongarra, J. M. Squyres, V. Sahay, P. Kambadur, B. Barrett, A. Lumsdaine, R. H. Castain, D. J. Daniel, R. L. Graham, and T. S. Woodall: EuroPVM/MPI: European MPI Users' Group Meeting. (2004) 97.

[44] W. Gropp, E. Lusk, and A. Skjellum: "Using MPI: Portable Parallel Programming with the Message Passing Interface", (MIT Press, 1999) 13.

[45] P. Balaji, D. Buntinas, D. Goodell, W. Gropp, S. Kumar, E. Lusk, R. Thakur, and J. L. Träff: 19th European MPI Users' Group Meeting. (2009) 20.

[46] G. M. Amdahl: Proceedings of the Spring Joint Computer Conference. (1967) 483.

[47] J. L. Gustafson: Commun. ACM, 31, (1988) 532.

(Received: June 13, 2024, Accepted: January 19, 2025)